Aging effect on lithium-ion battery resistance hysteresis

Simone Barcellona, Silvia Colnago, *Graduate Student Member, IEEE*, and Luigi Piegari, *Senior Member, IEEE*

***Abstract*— In recent years, lithium-ion batteries have been broadly employed in many different applications that require high energy and power density. In both static and mobile applications, the onboard estimation of internal parameters such as the capacity and internal resistance is of paramount importance. In particular, the internal resistance of a battery limits the power it can deliver and affects the overall efficiency. The battery resistance changes under different conditions, such as temperature, state of charge, and aging. In addition, a hysteresis resistance phenomenon was discovered and analyzed for different temperatures in a previous work. Indeed, the internal resistance of a battery changes based on the charging or discharging phase for a fixed state of charge and temperature. In the present work, the hysteresis phenomenon was deeply analyzed, even considering the cycle aging of the battery. To do this, several tests were performed using the electrochemical impedance spectroscopy method. Finally, a mathematical model capable of predicting how the hysteresis changes as a function of aging, for a fixed state of charge and temperature, was proposed.**

***Index Terms*— aging of lithium-ion batteries, battery internal resistance, hysteresis.**

I. INTRODUCTION

NOWADAYS the increasing use of renewable energy sources with intermittent electric production (e.g., photovoltaic panels and wind turbines), small mobile devices (e.g., smartphones and laptops), and traction applications (e.g., electric vehicles and railway traction) has produced an increasing need for energy storage systems, particularly batteries. Among the different technologies, lithium-ion batteries (LiBs) are the most used, thanks to their high energy density, medium power density, high efficiency, and relatively long lifecycle [1]–[4].

In all the aforementioned applications, both the energy and power delivered by the batteries are of fundamental importance. For these reasons, the aging analyses are focused on the internal resistance of a battery, which affects the maximum available power, and on its capacity, which affects the maximum available energy.

To properly control a battery, improve its efficiency, and reduce its degradation, it is essential to construct accurate models of the battery itself. This will make it possible to estimate the behavior of the battery under specific working conditions and predict its internal resistance and capacity variations. The present work analyzed the behavior of the internal resistance of a battery.

There are four main contributions to the internal resistance of a LiB [5]. The first is the high-frequency resistance, which is mainly related to the electronic and ionic resistances of the current collectors, electrodes, electrolyte, and separator. The second is the resistance of the solid electrolyte interface (SEI), which is related to its formation [6]. This interface is formed in the first charge/discharge cycles and continues to be modified during the battery lifetime [6]. The third is the charge transfer resistance, which is related to the charge transfer processes of chemical reactions [7], [8]. Finally, the last contribution is the diffusion resistance, which is related to the diffusion processes of the mass transport limitations of the electrodes and electrolytes [9], [10].

In the literature, it is possible to find many methods to estimate the internal resistance of a battery. These can be classified into two main groups: time-domain methods such as the DC pulse technique and frequency-domain methods such as electrochemical impedance spectroscopy (EIS). The former imposes a current pulse, and the related voltage change is measured in a specific time step [5]. The latter injects a sinusoidal current (galvanostatic EIS) or voltage (potentiostatic EIS) signal with a small amplitude and evaluates the internal impedance at different frequencies. These are more straightforward and accurate methods but require expensive equipment [11]. Nonetheless, in this study, galvanostatic EIS (GEIS) was used to estimate the internal resistance of a battery under different working conditions.

According to the literature, the internal resistance of a battery depends on different factors such as the temperature, state of charge (SOC), and current rate. In [12] and [13], the authors used EIS to analyze the variation of a battery's internal resistance as a function of the temperature and SOC. Several experiments were conducted at different temperatures (at a fixed SOC) and different SOCs (at a fixed temperature) to separately analyze the influences of the temperature and SOC. A very strong dependence on the temperature was found for all the resistance contributions. On the other hand, the SOC seemed to mainly affect the charge transfer and diffusion resistances. In [5], the authors used the DC pulse method to obtain similar results concerning the different contributions of the internal resistance variations as a function of the SOC and temperature. Moreover, in [5], the DC pulse method was used with different current amplitudes and pulse durations in order to take into account the influences of these parameters on the internal resistance values. In particular, the authors showed

Simone Barcellona, Silvia Colnago, and Luigi Piegari are with the Department of Electronics, Information and Bioengineering, Politecnico di Milano, Piazza Leonardo da Vinci, 32, 20133 Milano, Italy (email: simone.barcellona@polimi.it, silvia.colnago@polimi.it, luigi.piegari@polimi.it).

that the charge transfer resistance was strongly dependent on the current amplitude, and it decreased as the current increased. In [14], in addition to the DC pulse methods, the voltage curve difference and dynamic resistance methods were employed to show the influences of the SOC and current rate on the internal resistance of four different LiB cells. The authors stated that the high-frequency resistance was not affected by those factors. On the other hand, the charge transfer and diffusion resistances were dependent on the SOC and current rate.

LiBs are subjected to degradations by different mechanisms both when they are stored (calendar aging) and when they are used (cycle aging), affecting their state of health (SOH). In calendar aging, the SOC and temperature are the main factors that affect the SOH as a function of time [15], [16]. In cycle aging, the main factors that affect the SOH are the total moved charge, cut-off voltages, and current rate [16]–[18]. In both cases, according to the aging mechanism, the SOH of a battery can involve a capacity decrease (energy fade) or resistance increase (power fade). Therefore, the capacity or internal resistance is taken as an indicator of the SOH. Focusing on how the internal resistance of a battery depends on aging, in [19], the authors showed that the internal resistance changed as a function of the calendar aging for different temperatures and SOC levels. In particular, an increase in the internal resistance was accelerated exponentially by increasing the temperature or SOC level. Similarly, in [20], the authors showed the internal resistance trend as a function of calendar aging. Moreover, they analyzed the impact of cycle aging on the internal resistance increase.

In all the aforementioned works, a single internal battery resistance value was measured under certain temperature, SOC, and SOH conditions, without considering whether it was measured after a charging or discharging phase. On the other hand, in [21], the authors used the EIS method to analyze the internal battery resistance of an LiB during both the charging and discharging phases for different temperature and SOC values. The results showed that under all the investigated working conditions, the internal battery resistances estimated during the charging and discharging phases were different, which was the first demonstration of the hysteresis phenomenon called resistance hysteresis. Nevertheless, how this phenomenon changed as a function of aging was not analyzed.

This hysteresis phenomenon can be very interesting, in real applications, for the correct evaluation of the internal resistance for battery modeling as well as for SOC and SOH estimation. Indeed, if such a phenomenon is not considered, the estimated value of the internal resistance can be interpreted in an incorrect way leading to wrong SOC and SOH estimations.

In the light of the above, in the present study, based on the results reported in [21], analyses of the resistance hysteresis phenomenon were performed under different temperatures, while considering the battery cycle aging. In particular, an LiB cell was cycled under fixed working conditions (SOC range, temperature, and current rate). The internal resistance was estimated for the fresh LiB cell under test and after each aging cycle. In this way, it was possible to assess how the resistance hysteresis phenomenon changed as a function of the total moved charge. Finally, a simple mathematical model was proposed to predict the internal battery resistance hysteresis, for different temperatures, as a function of the cycle aging.

II. Battery Equivalent Model

The electrical circuit model is widely used in the literature because it assures a good trade-off between accuracy and complexity [22]. Different equivalent circuits can be employed, depending on the physical properties to be analyzed and the required precision. The electrical battery model typically includes a voltage source representing the open circuit voltage (OCV) in series with an impedance. Generally, the OCV depends on the SOC, temperature, and SOH, as well as on whether the battery is in the charging or discharging phase (voltage hysteresis) [23], [24]. In contrast, the internal impedance models the internal losses and dynamic response of the battery cell. A very common equivalent electric circuit model used in the literature is the one depicted in Fig. 1. The internal impedance consists of a series of four different impedances, each representing one of the four different effects occurring inside the cell [5]. The first contribution is the high-frequency resistance, R_s (ohmic resistance). The second contribution is the RC parallel branch, which is composed of the resistance, R_{SEI}, and capacitance, C_{SEI}, related to the SEI. The third contribution is the RC parallel branch composed of the resistance, R_{ct}, related to the charge transfer polarization, and the capacitance, C_d, related to the double-layer capacitance effect [22]. The last contribution is the Warburg impedance, Z_W, related to the diffusion process and mass transfer limitations.

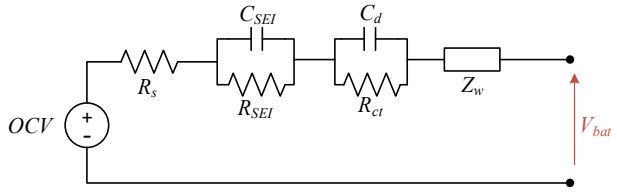

Fig. 1. Battery equivalent circuit

In this study, we were interested in investigating the hysteresis phenomenon for the internal battery resistance. To thoroughly analyze the phenomenon, both the high- and low-frequency resistances were investigated at different SOCs and temperatures. From a physical point of view, the low-frequency resistance should be considered as the sum of all four resistance terms. Consequently, to take into account even the diffusion resistance term, the GEIS should be performed up to very low frequencies. This is difficult because such tests at very low frequencies would be too long, and the total charge exchanged with the battery could move the SOC sufficiently out of the working condition under the analysis to provoke nonlinear effects and thus giving wrong results.

On the other hand, the time constant in the range of interest for the power calculation can be related to the local minimum of the second semicircle [25].

From a practical point of view, to obtain the value of R_s, the GEIS was performed at different SOCs and temperatures, and for each test, the intersection of the battery response with the real axis was considered. Analogously, to obtain R_{LF}, the real part of the local minimum of the equivalent impedance was considered. For better clarity, the two points are marked in Fig. 2.

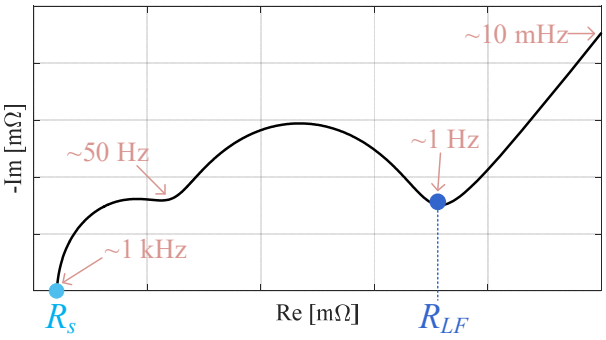

Fig. 2. Battery impedance spectrum

III. Test Setup and Procedure

A. Cell characteristics and test setup

The cell under study was a $LiCoO_2$ cell (8773160K), manufactured by General Electronics Battery Co. Ltd, whose main data are listed in Table 1. Nevertheless, the proposed procedure is general and can be applied also to other battery chemistries.

TABLE I
Cell Parameters

Parameter	Value [Unit]
Nominal capacity	10 [Ah]
Charge cut-off voltage	4.2 [V]
Discharge cut-off voltage	2.75 [V]
Maximum continuous current	100 [A]

The test setup used in this study is the one employed in [21].

B. Test procedure

The test procedure could be divided in two phases: the cycle aging phase and resistance calculation phase. The resistance calculation was performed at the beginning of the test and for every 5000 Ah of moved charge, until 20000 Ah.

During the aging cycles, the temperature was kept constant at around 30 °C. To speed up the test, a current of 50 A (5C) was chosen, because such a current rate, under constant temperature conditions, did not influence the aging [26]. Because of the cycle aging, the capacity of the LiB cell decreased, and after moving 10000 Ah, the aging cycles at 50 A only lasted a short time, causing an aging difference due to the high-frequency effect [27]. To avoid that effect, the current was decreased to 40 A (4C). The charge and discharge cycles were limited by the SOC boundaries (20–80 %) and voltage boundaries (3.45–4.05 V). Because of the high current employed for the tests, the voltage boundaries were reached before the SOC ones. Therefore, the charge moved in each cycle was less than the expected 6 Ah. However, according to [28], the aging of the battery did not depend on the shape of the aging cycle but just on the moved charge. Despite in this case the aging temperature was chosen to be 30 °C and the SOC limits were chosen in the linear battery range, the cycle aging phase can be performed at different aging conditions, such as different temperatures or SOC boundaries.

The LiB cell resistances were tested at five different temperatures ranging from 20 °C to 40 °C in steps of 5 °C. The LiB cell was cooled down to 20 °C and charged to 100% of the SOC using a constant current/constant voltage protocol: the LiB cell was charged with a current of 10 A (1C) until it reached the cut-off charging voltage (4.2 V), and then the cut-off voltage was applied until the current rate decayed to 100 mA (0.01C). When the charge was completed, the LiB cell was left to rest for 1 h, and then a GEIS was performed. Afterward, the LiB cell was discharged with a current of 10 A to 75% of the SOC, and after 1 h of rest, another GEIS was performed. This procedure was repeated, discharging 25% of the SOC at each step until the 0% condition was reached. At 0% of the SOC, another GEIS was performed after 1 h of rest, and then the same procedure was repeated in charging. After reaching 100% of the SOC, the LiB cell temperature was increased by 5 °C, and the same procedure was repeated.

IV. Results of New Battery Hysteresis

As discussed above, the high- and low-frequency battery internal resistance values were obtained by considering the GEIS results. As reported in [21], for both the high- and low-frequency resistances, it was possible to note a difference between the resistance values evaluated during the charging and discharging phases. In fact, for the same temperature and SOC level, there were two different resistance values, and, in general, the resistance evaluated during the discharging phase was higher than that evaluated during the charging phase. This behavior could be interpreted as the *resistance hysteresis*, and it was wider in the center of the curve, i.e., between 40% and 80% of the SOC. This hysteresis did not depend on the voltage at which it was evaluated, but depended on the condition of the battery before the measurement, i.e., in the charge or discharge state. Indeed, as discussed in [21], the resistance values during charging and discharging were different even if the voltage at which they were evaluated differed by a few millivolts.

The modified Akima cubic Hermite interpolation was used to determine the values of the two resistance curves for every 5% change in the SOC. This gave the interpolated values based on a piecewise function of polynomials with a degree of at most three to avoid local undulations, especially when quick changes occurred between flat regions. The results for the high- and low-frequency resistances of the fresh LiB cell, with their interpolations, are reported in Fig. 3 and Fig. 4, respectively. The absolute value of the differences between the resistances measured during the discharging and charging of the fresh battery, here called the width of the hysteresis, are reported in Fig. 7a and Fig. 8a, for the high- (ΔR_S) and low-frequency (ΔR_{LF}) resistances, respectively. As already

discussed in [21] and highlighted in Fig. 7a and Fig. 8a, the width of the hysteresis decreased with increasing temperature for both the high- and low-frequency resistances. However, the low-frequency resistance showed a slightly larger hysteresis at 25 °C with respect to 20 °C between 65% and 95% of the SOC. For both the high- and low-frequency resistances, at a high temperature (40 °C), the resistance hysteresis was very small, and for an SOC greater than 80% or 70%, respectively, the resistance during discharging was greater or equal to the resistance during charging.

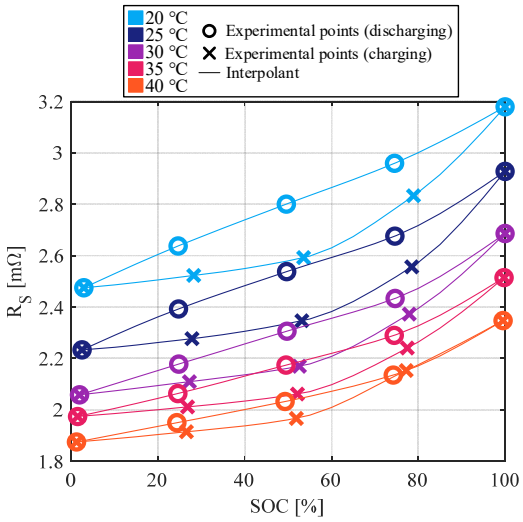

Fig. 3. Results for high-frequency resistance of fresh cell

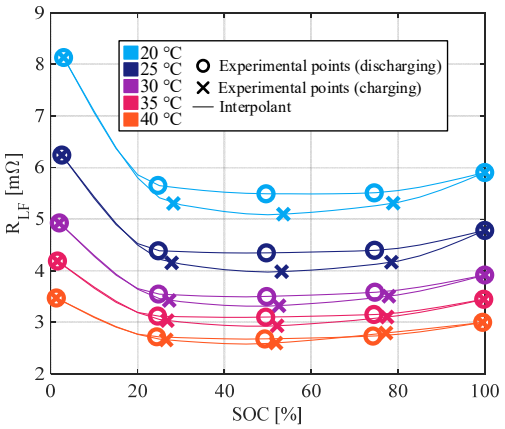

Fig. 4. Results for low-frequency resistance of fresh cell.

V. Results of Hysteresis Dependency on Aging

To test the behavior of the resistance hysteresis as a function of the cycle aging of the battery, the same tests performed on the fresh LiB cell were repeated for every 5000 Ah of moved charge. It is well known that cycle aging affects both the capacity and resistance of an LiB cell. In particular, the latter increases with the moved charge [29], which could also affect the hysteresis phenomenon. In the following, the results of the high- and low-frequency resistances are reported to analyze this aspect, and a mathematical model of the phenomenon is proposed.

A. High- and low-frequency resistance results

The results for the high- and low-frequency resistances as a function of the cycle aging under different temperatures are reported in Fig. 5 and Fig. 6, respectively, together with the interpolations obtained using the modified Akima cubic Hermite interpolation. This was used to obtain a value for every 5% of the SOC, and the related widths of the hysteresis were computed.

In order to highlight the different trends for the resistance hysteresis, as a function of aging and temperature, the ΔR_S and ΔR_{LF} values are shown in two ways. Fig. 7 (for ΔR_S) and Fig. 8 (for ΔR_{LF}) show, in each subplot, the results for different temperatures at every age, while Fig. 9 (for ΔR_S) and Fig. 10 (for ΔR_{LF}) show, in each subplot, the results at different ages at each temperature.

From Fig. 7 and Fig. 8, it is possible to recognize that the decreasing trend of the hysteresis width with increasing temperature, already discussed for the fresh cell, became less evident with increasing age. On the other hand, it is possible to note that for low temperatures (20–25 °C) the width was basically larger than for high temperatures (35–40 °C) at every age. Conversely, looking at Fig. 9 and Fig. 10, where the same results are reported for different ages and a fixed temperature, it is not possible to identify a clear trend for the hysteresis width as a function of the aging. However, the variation of the hysteresis width was limited between 0.1 mΩ and 0.2 mΩ. Therefore, it could be said that the effect of the cycle aging on the width of the hysteresis was negligible. In other words, the width remained practically constant as a function of the moved charge for almost all the temperatures. This means that for a fixed temperature, the hysteresis cycle moved upward, maintaining an almost constant area.

Finally, at high temperatures and high SOCs, unlike the results in the other cases, both the high- and low-frequency resistances evaluated during charging is higher than the one evaluated during discharging. This can be seen in Fig. 5 and Fig. 6, where the curves of the charging and discharging resistances intersect with each other. This phenomenon may have been due to the fact that the experimental points (in charging and discharging) were very close to each other, meaning that the hysteresis was very tight. For the low-frequency resistance, it is possible to note a similar trend for a low SOC at each temperature. In the authors' opinion, the latter intersections may have been due to the large discretization of the experimental points and to a consequent error of the interpolating function.

B. Model

As shown in the results (Fig. 5 and Fig. 6), the resistances under the same conditions for the SOC, temperature, and charging or discharging phase increased with the moved charge. The aim was to find a mathematical law capable of predicting this behavior, which was the same for all the aforementioned conditions, in order to obtain a mathematical model of the resistance increase trend that also considers the hysteresis phenomenon. The following shows a mathematical law that predicts the value of the internal battery resistance, as a function of the moved charge, for a fixed temperature, SOC,

and charging or discharging phase, starting from the resistance value of the fresh battery cell:

$$R(Q) = \alpha \cdot Q^{0.7} + \beta \cdot Q + \gamma \quad (1)$$

where Q is the total moved charge, and α, β, and γ are the fitting coefficients. This means that, for each SOC and temperature level, both the high- and low-frequency resistances increase with a linear term and 0.7th fractional order term, whose coefficients depend on the working conditions. The fitting results for the high- and low-frequency resistances are reported in Fig. 11 and Fig. 12, respectively. Moreover, it is possible to normalize (1) by dividing it by the γ coefficient that represents the resistance value of the fresh cell:

$$R_{pu}(Q) = \alpha_{pu} \cdot Q^{0.7} + \beta_{pu} \cdot Q + 1 \quad (2)$$

where the normalized coefficients (α_{pu} and β_{pu}) are reported in the appendix.

Finally, the model shows a good agreement with the experimental data. Fig. 13 and Fig. 14 report the percentage error, which can be calculated as follows:

$$\varepsilon = \frac{R^* - R_{meas}}{R_{meas}} \cdot 100 \quad (3)$$

where R^* is the resistance calculated by the model, and R_{meas} is the corresponding experimental value. For the high-frequency resistance, the model can predict the value of the aged resistance with a maximum error of 2%, while the low-frequency resistance prediction has a maximum error of 7%. It is worth noting that, while the high-frequency resistance is precisely defined by the intersection of the Nyquist diagram with the real axis (see Fig. 2.), the low-frequency resistance, as previously discussed, was estimated with an approximation, which can partially explain the higher error of the model.

VI. PRACTICAL IMPLICATIONS

The estimation of battery parameters, such as SOC and SOH, is of paramount importance in many battery applications ranging from electric vehicles (EV) to mobile phones, besides the application of storage together with renewable energy sources. The SOC estimation can be performed using different methods, among them, the model-based one relies on the equivalent circuit battery parameters, including the internal resistance. The SOH estimation is usually related to two main indicators: energy and power fade. The latter is evaluated through the internal resistance increase.

As analyzed in [21] and in this paper, the internal battery resistance values evaluated during the charge and discharge phase, for the same SOC, temperature, and aging conditions, are different due to the hysteresis phenomenon. Consequently, the latter, if not considered, can lead to a wrong estimation of SOC or SOH.

In EV, the SOC estimation is related to the information on the vehicle range. The reliability of this information is crucial to reduce the range-anxiety of the drivers which is one of the obstacles to the diffusion of EVs. The SOH indicates the reduction of the battery capacity and, therefore, its correct estimation is necessary for two main reasons: i) to correctly estimate the SOC in aged vehicles; ii) to provide predictive maintenance to substitute the battery pack of the EV without causing an undesired stop of the vehicle itself.

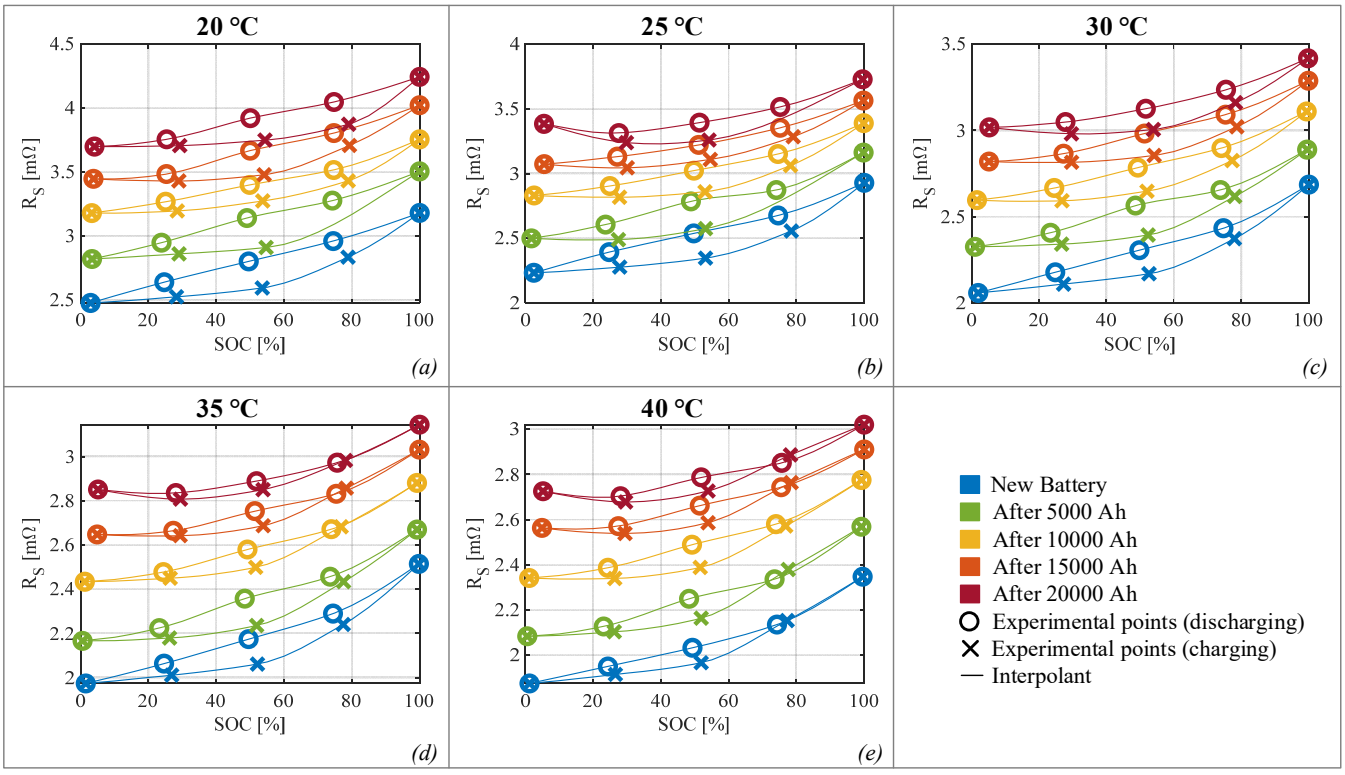

Fig. 5. Results for high-frequency resistance as a function of aging for different temperatures

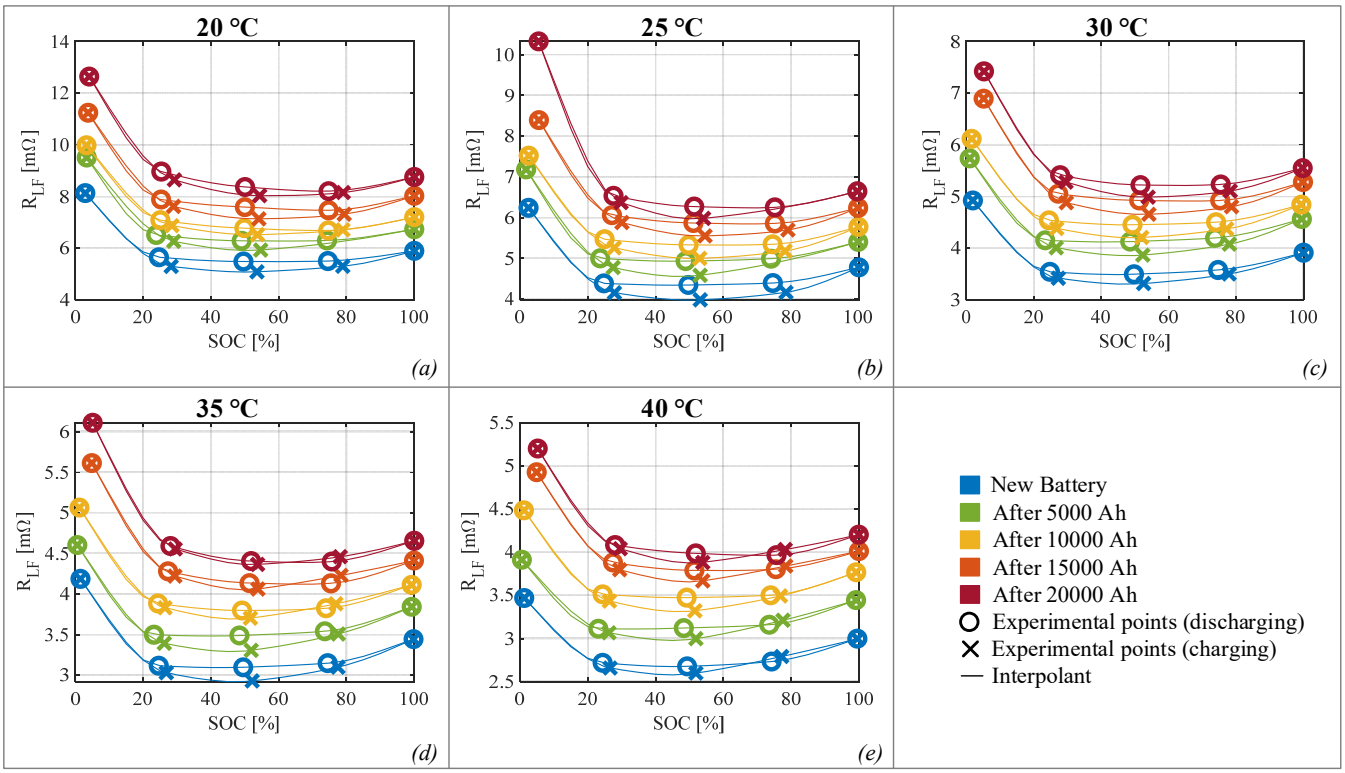

Fig. 6. Results for low-frequency resistance as a function of aging for different temperatures

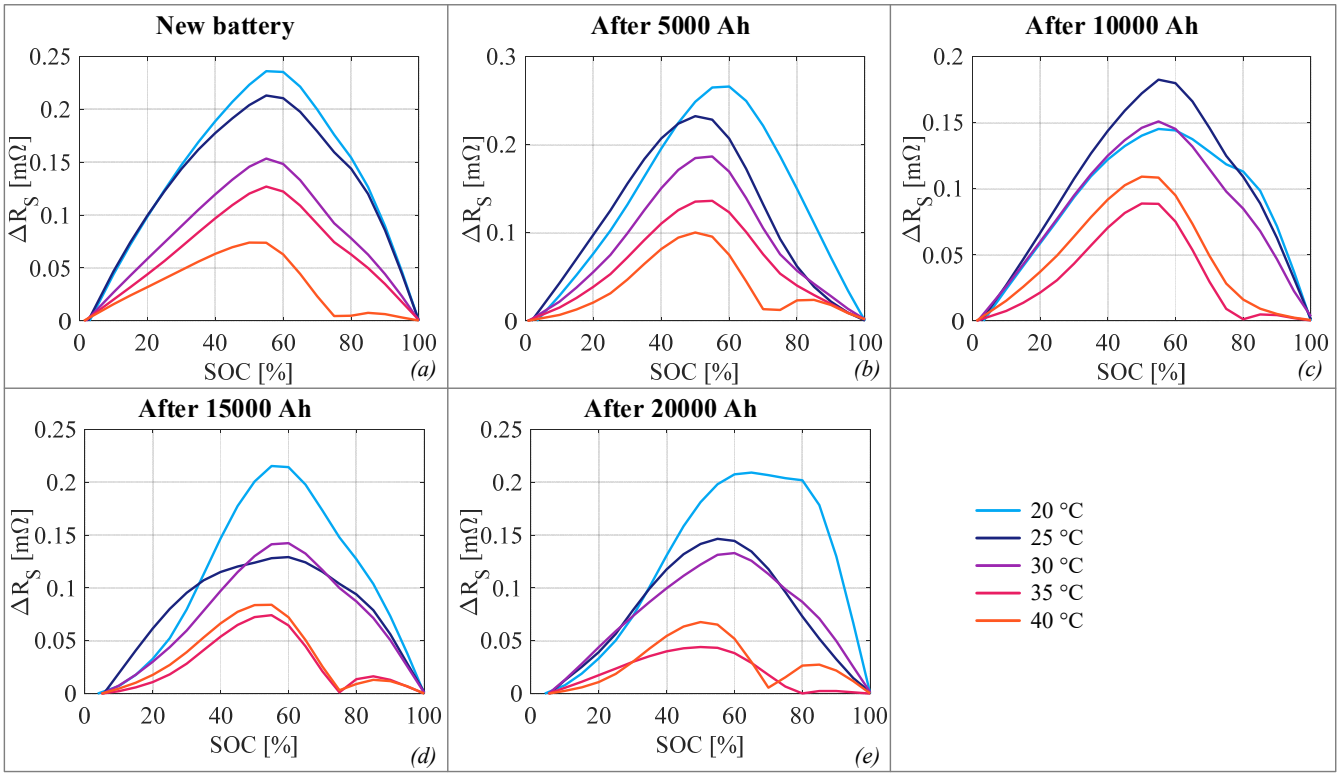

Fig. 7. Width of the high-frequency hysteresis as a function of temperature for different ages

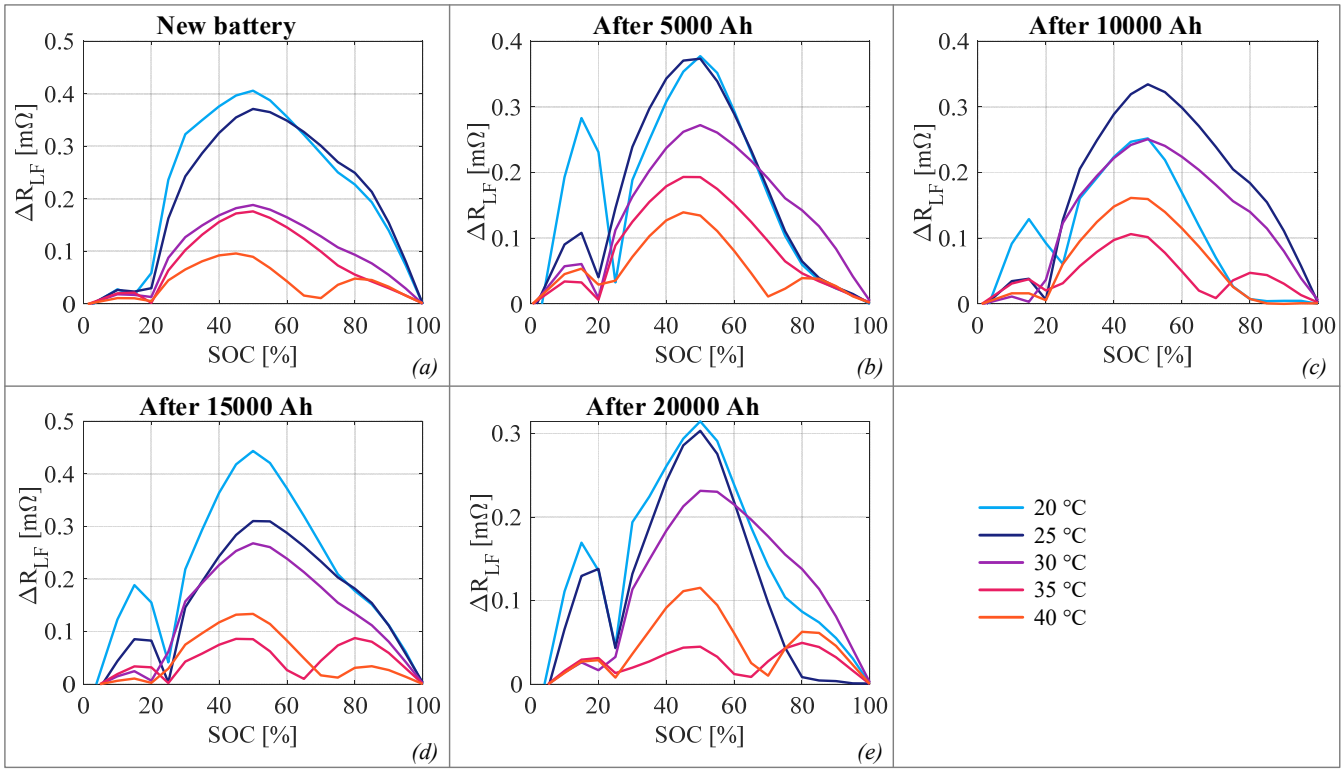

Fig. 8. Width of the low-frequency hysteresis as a function of temperature for different ages

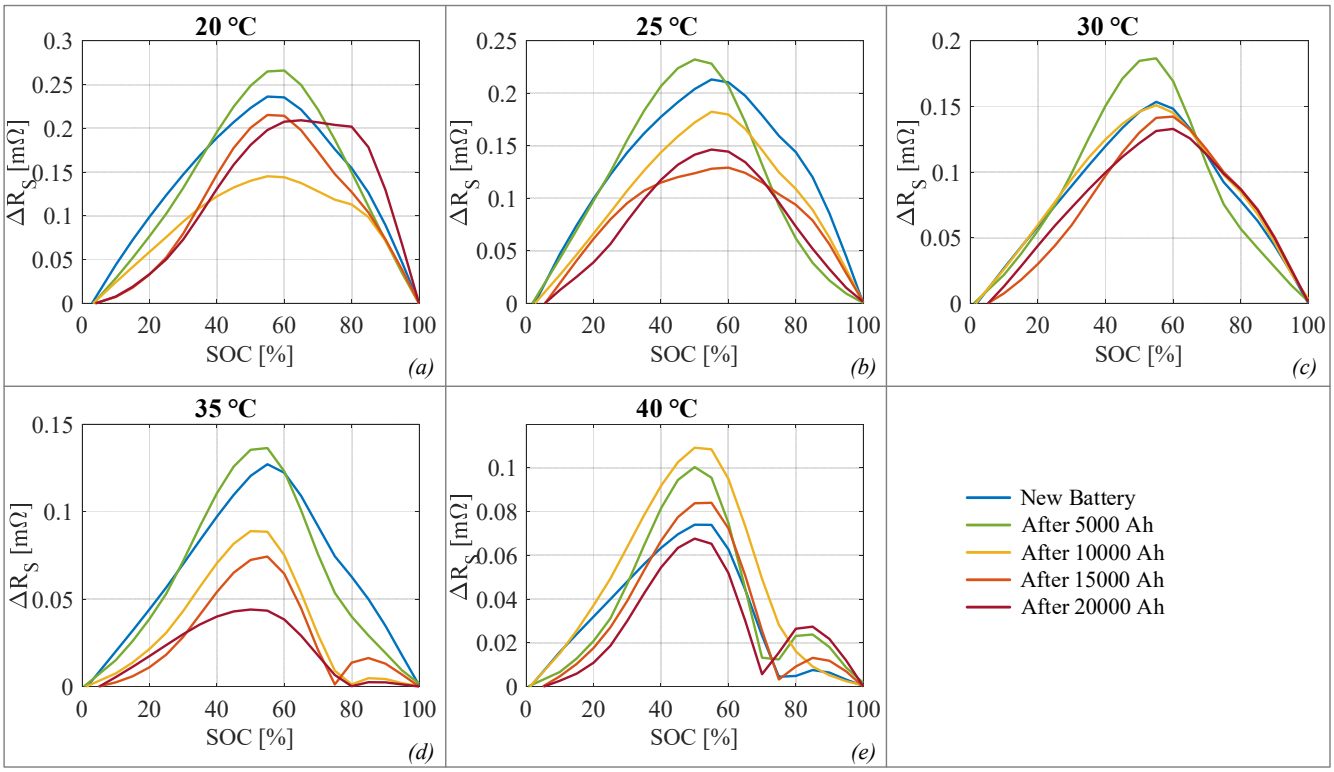

Fig. 9. Width of the high-frequency hysteresis as a function of aging for different temperatures

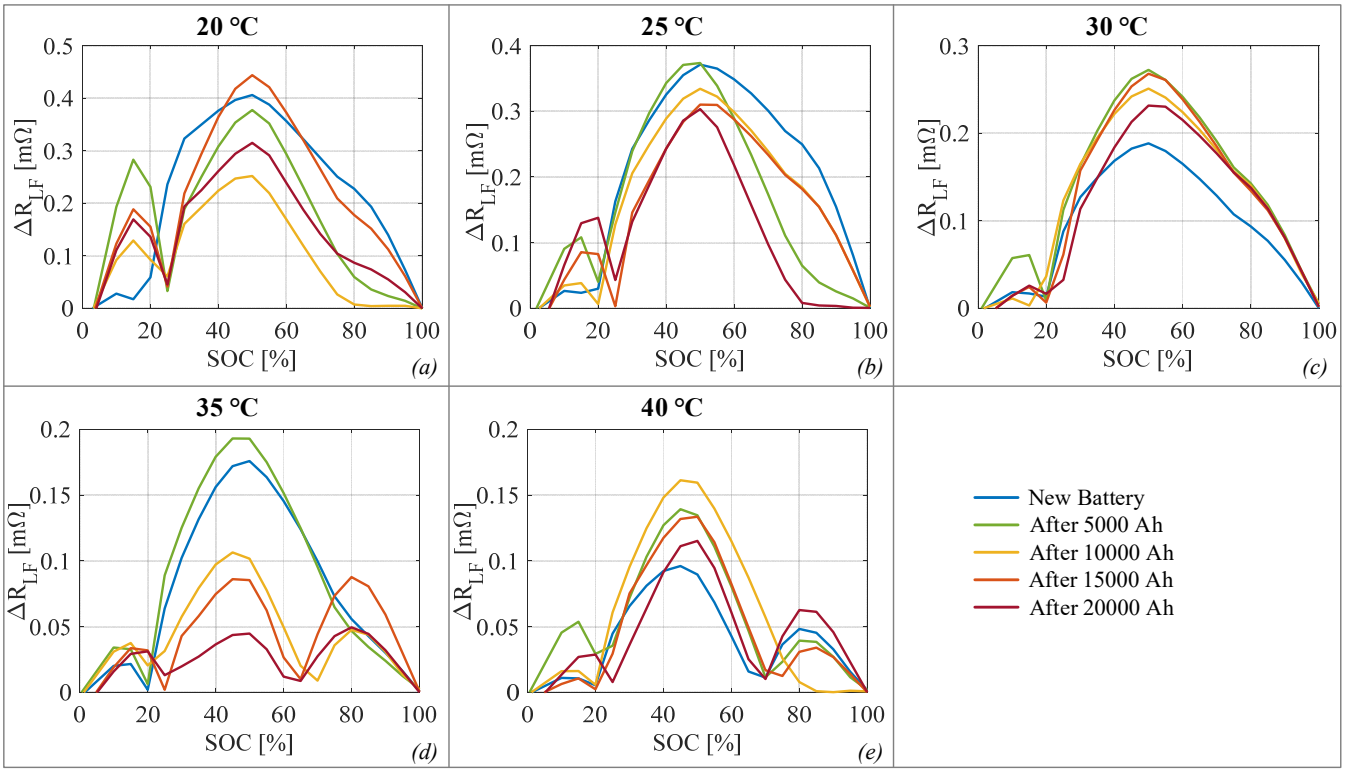

Fig. 10. Width of the low-frequency hysteresis as a function of aging for different temperatures

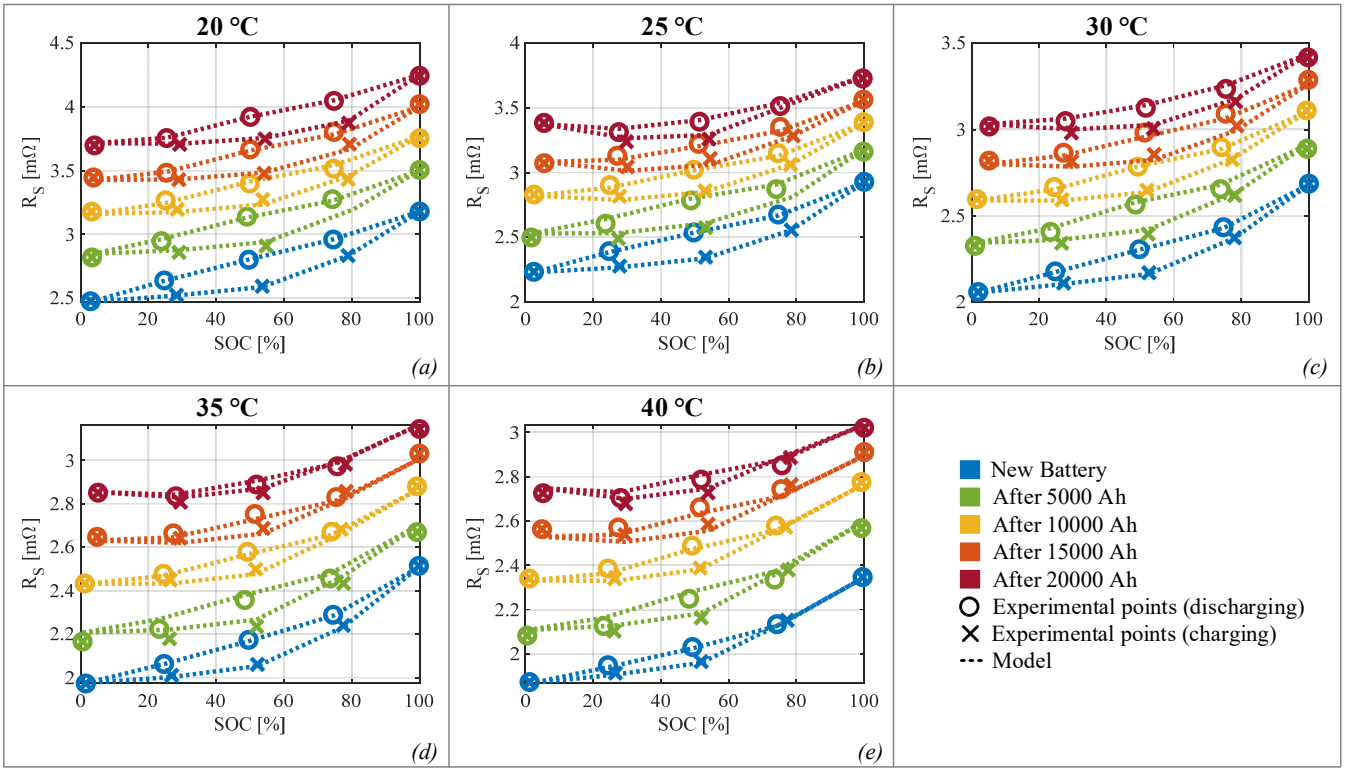

Fig. 11. Results for high-frequency resistance as a function of aging for different temperatures with the related fitting curves

This article has been accepted for publication in IEEE Transactions on Industry Applications. This is the author's version which has not been fully edited and content may change prior to final publication. Citation information: DOI 10.1109/TIA.2023.3266307

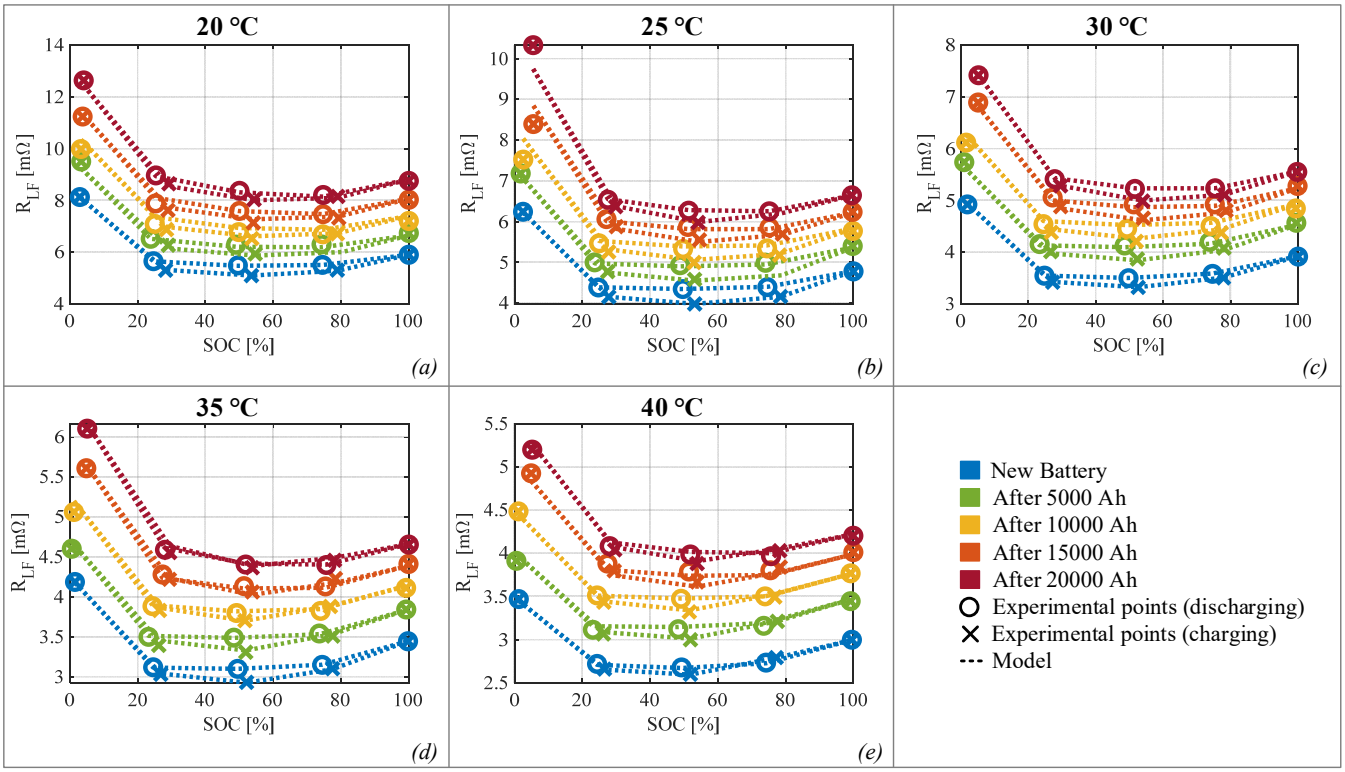

Fig. 12. Results for low-frequency resistance as a function of aging for different temperatures with the related fitting curves

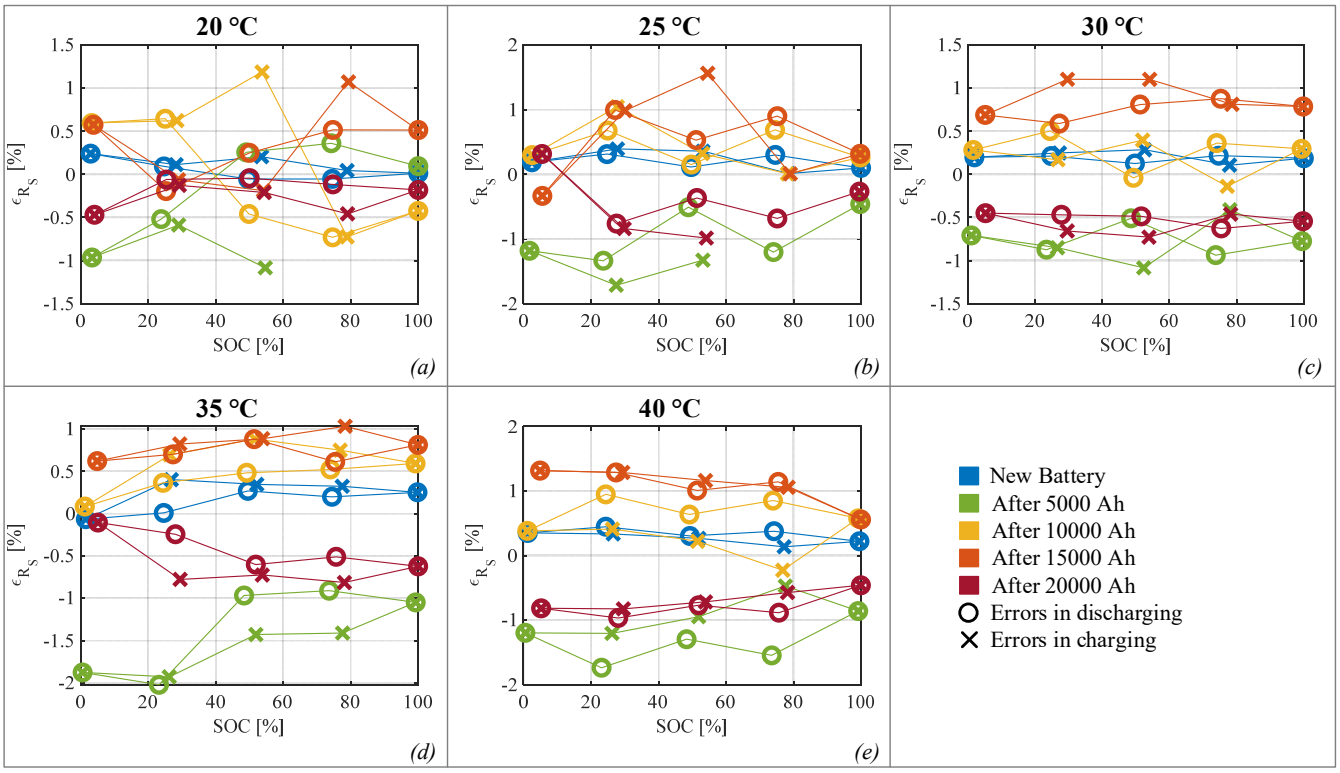

Fig. 13. Percentage error of high-frequency resistance as a function of aging for different temperatures

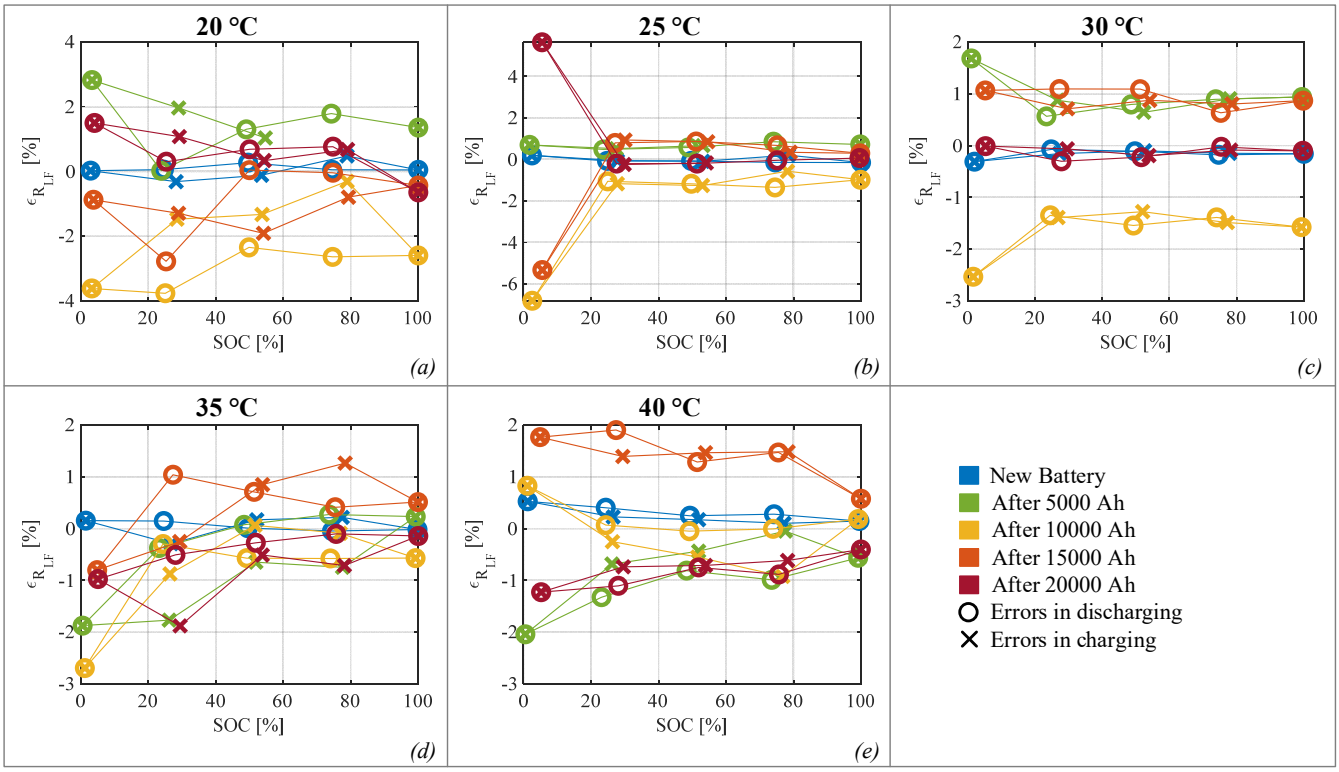

Fig. 14. Percentage error of low-frequency resistance as a function of aging for different temperatures

In mobile phones, the SOC estimation is not only important to give correct information to the user, but it can be used to optimize the charging phase to enlarge the lifetime of the battery itself.

In recent years, the application of batteries grid-connected is also spreading. In low voltage grids, batteries are used, at the house or building level, in combination with renewable energy sources (e.g., PV panels) to maximize the self-consumption minimizing the losses for energy transmission and distribution and building quasi-autonomous microgrids. The estimation of SOC and SOH is necessary for both a correct implementation of the self-consumption strategy and a safe use of the battery pack. In high voltage grids, batteries are used to support the grid mainly in voltage and frequency regulations. Again, the correct estimation of the SOC and SOH is necessary for the optimal use of the storage. Finally, in the energy market, both the SOC and SOH are used to define the strategy for the utilization of battery energy in the market itself.

It is worth noting that, a precise SOH estimation is particularly crucial in applications where the lack of power can result in safety issues. Not considering the resistance hysteresis can lead to an underestimation of the actual resistance, and the battery being used even if the end of life is already reached.

VII. Conclusion

In this study, the internal resistance of an $LiCoO_2$ battery cell was analyzed during the charging and discharging phases under different temperature, SOC, and cycle aging conditions. The latter was quantified using the total moved charge exchanged with the battery under test. The internal battery resistance was measured using the GEIS technique, and, according to [5], it was considered to be composed of four main terms: the high-frequency resistance, SEI resistance, charge transfer resistance, and diffusion resistance. Neglecting the last term, the high- and low-frequency resistances were derived from the spectroscopy results.

For the first time in [21], the authors showed that at the same SOC level and fixed temperature, a battery's internal resistances were different during the charging and discharging phases, claiming that a hysteresis resistance phenomenon occurred. Moreover, the hysteresis was more significant at low temperatures, while it became less evident with increasing temperature.

In the light of the above, in the present work, this phenomenon was deeply analyzed, while also considering the cycle aging of the battery. In particular, for a fresh LiB cell and after each cycle aging phase, the high- and low-frequency internal battery resistances were evaluated for different temperatures and SOCs.

The hysteresis phenomenon can be of great importance for battery modeling and correctly estimating battery parameters. In fact, if it is not considered, the value of the internal resistance can be evaluated differently according to the charge or discharge phase giving misleading results in terms of actual SOC and SOH.

From the results for different temperatures and fixed aging (Fig. 7 and Fig. 8), the trend of the resistance hysteresis width became less evident with increasing age, but at high temperatures it was smaller than at low temperatures.

On the other hand, for a fixed temperature (Fig. 9 and Fig. 10), it was not possible to derive a clear trend for the resistance hysteresis width as a function of aging. In fact, at each temperature, the resistance hysteresis widths seemed to be similar for different ages. Therefore, we considered the effect of the cycle aging on the hysteresis width to be negligible, i.e., the width remained almost constant with the moved charge. This means that for a fixed temperature, the hysteresis cycle moved upward, maintaining an almost constant area.

Finally, in addition to this analysis, a mathematical model was proposed, which could predict the high- and low-frequency resistances under certain conditions for the temperature, SOC, charging and discharging phase, and age, based on the resistance value of the related fresh cell. According to the proposed model, the internal resistance increases according to the same mathematical law for all the SOC and temperature levels but with different coefficients.

APPENDIX

In Table II-V, the normalized coefficient, α_{pu}, β_{pu}, for all the temperatures, SOC, and charging (ch) or discharging (dis) phase are reported.

TABLE II
COEFFICIENT α_{pu} OF R_s

SOC [%]	Temperature [°C]				
	20	25	30	35	40
100	1.16E-04	1.17E-04	1.06E-04	6.67E-05	2.37E-04
75dis	6.04E-05	4.71E-05	1.26E-04	4.56E-05	1.94E-04
50dis	1.18E-04	1.27E-04	2.02E-04	8.27E-05	2.01E-04
25dis	1.16E-04	3.62E-05	9.55E-05	2.42E-05	8.28E-05
0	1.82E-04	2.24E-05	1.42E-04	2.53E-05	6.12E-05
25ch	1.56E-04	2.89E-05	1.01E-04	2.50E-05	7.14E-05
50ch	1.61E-04	8.71E-05	1.27E-04	1.52E-05	8.56E-05
75ch	2.51E-04	1.47E-05	1.70E-04	1.28E-04	1.71E-04

TABLE III
COEFFICIENT β_{pu} OF R_s

SOC [%]	Temperature [°C]				
	20	25	30	35	40
100	1.17E-05	8.56E-06	9.32E-06	1.03E-05	3.20E-06
75dis	1.63E-05	1.47E-05	1.14E-05	1.38E-05	8.46E-06
50dis	1.50E-05	1.15E-05	8.64E-06	1.36E-05	9.89E-06
25dis	1.64E-05	1.92E-05	1.66E-05	1.86E-05	1.71E-05
0	1.71E-05	2.59E-05	1.76E-05	2.21E-05	2.16E-05
25ch	1.68E-05	2.17E-05	1.71E-05	2.04E-05	1.81E-05
50ch	1.54E-05	1.69E-05	1.44E-05	2.01E-05	1.66E-05
75ch	6.61E-06	1.94E-05	9.04E-06	1.16E-05	9.52E-06

TABLE IV
COEFFICIENT α_{pu} OF R_{LF}

SOC [%]	Temperature [°C]				
	20	25	30	35	40
100	0.00E+00	1.66E-04	3.65E-04	1.74E-04	4.09E-04
75dis	9.08E-06	1.30E-04	3.33E-04	1.49E-04	3.95E-04
50dis	9.13E-06	1.06E-04	3.36E-04	1.26E-04	3.82E-04
25dis	3.23E-05	5.88E-05	2.23E-04	3.47E-05	2.39E-04
0	0.00E+00	1.99E-06	1.06E-04	0.00E+00	1.72E-04
25ch	0.00E+00	4.48E-05	1.65E-04	8.32E-06	2.10E-04
50ch	3.95E-05	1.07E-04	2.15E-04	7.56E-05	2.41E-04
75ch	4.68E-06	7.59E-06	2.74E-04	2.09E-04	2.78E-04

TABLE V
COEFFICIENT β_{pu} OF R_{LF}

SOC [%]	Temperature [°C]				
	20	25	30	35	40
100	2.60E-05	1.18E-05	2.96E-06	9.56E-06	3.21E-07
75dis	2.48E-05	1.54E-05	6.85E-06	1.32E-05	4.10E-06
50dis	2.68E-05	1.79E-05	8.56E-06	1.59E-05	6.67E-06
25dis	2.90E-05	2.29E-05	1.63E-05	2.36E-05	1.52E-05
0	2.80E-05	2.96E-05	2.09E-05	2.50E-05	1.87E-05
25ch	3.20E-05	2.59E-05	2.00E-05	2.73E-05	1.72E-05
50ch	2.80E-05	2.10E-05	1.53E-05	2.24E-05	1.42E-05
75ch	2.78E-05	2.55E-05	9.76E-06	1.29E-05	9.45E-06

REFERENCES

[1] K. C. Divya and J. Østergaard, "Battery energy storage technology for power systems—An overview," *Electric Power Systems Research*, vol. 79, no. 4, pp. 511–520, Apr. 2009, doi: 10.1016/j.epsr.2008.09.017.

[2] B. Diouf and R. Pode, "Potential of lithium-ion batteries in renewable energy," *Renewable Energy*, vol. 76, pp. 375–380, Apr. 2015, doi: 10.1016/j.renene.2014.11.058.

[3] S. Pelletier, O. Jabali, G. Laporte, and M. Veneroni, "Battery degradation and behaviour for electric vehicles: Review and numerical analyses of several models," *Transportation Research Part B: Methodological*, vol. 103, pp. 158–187, Sep. 2017, doi: 10.1016/j.trb.2017.01.020.

[4] M. A. Divakaran *et al.*, "Rational design on materials for developing next generation lithium-ion secondary battery," *Progress in Solid State Chemistry*, vol. 62, p. 100298, Jun. 2021, doi: 10.1016/j.progsolidstchem.2020.100298.

[5] B. V. Ratnakumar, M. C. Smart, L. D. Whitcanack, and R. C. Ewell, "The impedance characteristics of Mars Exploration Rover Li-ion batteries," *Journal of Power Sources*, vol. 159, no. 2, pp. 1428–1439, Sep. 2006, doi: 10.1016/j.jpowsour.2005.11.085.

[6] V. A. Agubra and J. W. Fergus, "The formation and stability of the solid electrolyte interface on the graphite anode," *Journal of Power Sources*, vol. 268, pp. 153–162, Dec. 2014, doi: 10.1016/j.jpowsour.2014.06.024.

[7] J. Li, E. Murphy, J. Winnick, and P. . Kohl, "Studies on the cycle life of commercial lithium ion batteries during rapid charge–discharge cycling," *Journal of Power Sources*, vol. 102, no. 1–2, pp. 294–301, Dec. 2001, doi: 10.1016/S0378-7753(01)00821-7.

[8] S. S. Zhang, K. Xu, and T. R. Jow, "Electrochemical impedance study on the low temperature of Li-ion batteries," *Electrochimica Acta*, vol. 49, no. 7, pp. 1057–1061, Mar. 2004, doi: 10.1016/j.electacta.2003.10.016.

[9] G. Ning, B. Haran, and B. N. Popov, "Capacity fade study of lithium-ion batteries cycled at high discharge rates," *Journal of Power Sources*, vol. 117, no. 1–2, pp. 160–169, May 2003, doi: 10.1016/S0378-7753(03)00029-6.

[10] T. B. Reddy and D. Linden, *Linden's Handbook of Batteries*, Fourth Edi. New York, NY: McGraw-Hill Education, 2011.

[11] H. G. Schweiger *et al.*, "Comparison of Several Methods for Determining the Internal Resistance of Lithium Ion Cells," *Sensors*, vol. 10, no. 6, pp. 5604–5625, 2010, doi: 10.3390/s100605604.

[12] D. Andre *et al.*, "Characterization of high-power lithium-ion batteries by electrochemical impedance spectroscopy. II: Modelling," *Journal of Power Sources*, vol. 196, no. 12, pp. 5349–5356, Jun. 2011, doi: https://doi.org/10.1016/j.jpowsour.2010.12.102.

[13] J. Gomez, R. Nelson, E. E. Kalu, M. H. Weatherspoon, and J. P. Zheng, "Equivalent circuit model parameters of a high-power Li-ion battery: Thermal and state of charge effects," *Journal of Power Sources*, vol. 196, no. 10, pp. 4826–4831, 2011, doi: https://doi.org/10.1016/j.jpowsour.2010.12.107.

[14] D. Anseán, V. M. García, M. González, J. C. Viera, C. Blanco, and J. L. Antuña, "DC internal resistance during charge: Analysis and study on LiFePO<inf>4</inf> batteries," in *2013 World Electric Vehicle Symposium and Exhibition (EVS27)*, 2013, pp. 1–11, doi: 10.1109/EVS.2013.6914746.

[15] K. Nunotani *et al.*, "Development and performance evaluation of lithium iron phosphate battery with superior rapid charging performance - Second report: Evaluation of battery capacity loss characteristics," in *2011 IEEE Vehicle Power and Propulsion Conference*, Sep. 2011, pp. 1–4, doi: 10.1109/VPPC.2011.6042998.

[16] S. S. Choi and H. S. Lim, "Factors that affect cycle-life and possible degradation mechanisms of a Li-ion cell based on LiCoO2," *Journal of Power Sources*, vol. 111, no. 1, pp. 130–136, Sep. 2002, doi: 10.1016/S0378-7753(02)00305-1.

[17] K. Asakura, M. Shimomura, and T. Shodai, "Study of life evaluation methods for Li-ion batteries for backup applications," *Journal of Power Sources*, vol. 119–121, pp. 902–905, Jun. 2003, doi: 10.1016/S0378-7753(03)00208-8.

[18] H. Gong *et al.*, "Solvothermal synthesis of LiFePO4/C nanopolyhedrons and microellipsoids and their performance in lithium-ion batteries," *Materials Letters*, vol. 66, no. 1, pp. 374–376, Jan. 2012, doi: 10.1016/j.matlet.2011.08.093.

[19] D.-I. Stroe, M. Swierczynski, S. K. Kar, and R. Teodorescu, "Degradation Behavior of Lithium-Ion Batteries During Calendar Ageing—The Case of the Internal Resistance Increase," *IEEE Transactions on Industry Applications*, vol. 54, no. 1, pp. 517–525, Jan. 2018, doi: 10.1109/TIA.2017.2756026.

[20] M. Ecker *et al.*, "Calendar and cycle life study of Li(NiMnCo)O2-based 18650 lithium-ion batteries," *Journal of Power Sources*, vol. 248, pp. 839–851, Feb. 2014, doi: 10.1016/j.jpowsour.2013.09.143.

[21] S. Barcellona, S. Colnago, and L. Piegari, "Analysis of the lithium-ion batteries resistance hysteresis phenomenon," in *2022 International Symposium on Power Electronics, Electrical Drives, Automation and Motion (SPEEDAM)*, Jun. 2022, pp. 46–51, doi: 10.1109/SPEEDAM53979.2022.9842069.

[22] S. Barcellona and L. Piegari, "Lithium Ion Battery Models and Parameter Identification Techniques," *Energies*, vol. 10, no. 12, p. 2007, Dec. 2017, doi: 10.3390/en10122007.

[23] A. Farmann and D. U. Sauer, "A study on the dependency of the open-circuit voltage on temperature and actual aging state of lithium-ion batteries," *Journal of Power Sources*, vol. 347, pp. 1–13, Apr. 2017, doi: 10.1016/j.jpowsour.2017.01.098.

[24] F. Baronti, W. Zamboni, N. Femia, R. Roncella, and R. Saletti, "Experimental analysis of open-circuit voltage hysteresis in lithium-iron-phosphate batteries," in *IECON 2013 - 39th Annual Conference of the IEEE Industrial Electronics Society*, Nov. 2013, pp. 6728–6733, doi: 10.1109/IECON.2013.6700246.

[25] W. Waag, S. Käbitz, and D. U. Sauer, "Experimental investigation of the lithium-ion battery impedance characteristic at various conditions and aging states and its influence on the application," *Applied Energy*, vol. 102, pp. 885–897, Feb. 2013, doi: 10.1016/j.apenergy.2012.09.030.

[26] S. Barcellona and L. Piegari, "Effect of current on cycle aging of lithium ion batteries," *Journal of Energy Storage*, vol. 29, p. 101310, Jun. 2020, doi: 10.1016/j.est.2020.101310.

[27] M. Uno and K. Tanaka, "Influence of High-Frequency Charge–Discharge Cycling Induced by Cell Voltage Equalizers on the Life Performance of Lithium-Ion Cells," *IEEE Transactions on Vehicular Technology*, vol. 60, no. 4, pp. 1505–1515, May 2011, doi: 10.1109/TVT.2011.2127500.

[28] S. Barcellona, M. Brenna, F. Foiadelli, M. Longo, and L. Piegari, "Analysis of Ageing Effect on Li-Polymer Batteries," *The Scientific World Journal*, vol. 2015, pp. 1–8, 2015, doi: 10.1155/2015/979321.

[29] S. Barcellona, S. Colnago, G. Dotelli, S. Latorrata, and L. Piegari, "Aging effect on the variation of Li-ion battery resistance as function of temperature and state of charge," *Journal of Energy Storage*, vol. 50, p. 104658, Jun. 2022, doi: 10.1016/j.est.2022.104658.